Research Article

Journal of RAMAN SPECTROSCOPY

Received: 30 March 2009 Accepted: 14 July 2009 Published online in Wiley Interscience:

(www.interscience.wiley.com) DOI 10.1002/jrs.2438

Raman spectroscopy of synthetic, geological and biological vaterite: a Raman spectroscopic study

U. Wehrmeister,[a,b]* A. L. Soldati,[a] D. E. Jacob,[a] T. Häger[a,b] and W. Hofmeister[a,b]

Raman spectroscopy was used to study vaterite samples of biological, geological and synthetic origin. The Raman band positions and the full width at half-maximum (FWHM) of the lattice modes and the internal modes of the carbonate ion of all specimens show no significant differences between vaterites of different origin. With increasing Mg concentrations, synthetic vaterite samples show increasing FWHM in the region of the lattice modes and the three ν_1 bands, whereas no change in luminescence was detected. In contrast, *in situ* measurements of vaterite areas in freshwater cultured pearls (FWCPs) by laser ablation inductively coupled plasma mass spectrometry (LA-ICP-MS) together with the Raman spectra obtained at the same points show that the luminescence intensity in biological samples is affected by the magnesium content. The Raman spectroscopic features of vaterite and parisite-(Ce) are compared, and their similarities suggest that the structure of vaterite contains at least three crystallographically independent carbonate groups and similar carbonate group layers. A band at 263 cm^{-1} is observed for the first time in this study, whereas it could be demonstrated that bands previously reported at 130 and 190 cm^{-1} do not belong to vaterite.

Keywords: vaterite; freshwater cultured pearls; Raman spectra; parisite

Introduction

The pair aragonite and calcite are some of the most intensively studied polymorphic minerals. They are most commonly observed in biological minerals produced by marine molluscs,[1] whereas in freshwater molluscs mostly aragonite and vaterite (the third $CaCO_3$ polymorph) are identified.[2–6] Vaterite is the thermodynamically most unstable $CaCO_3$ polymorph and is often discussed as a precursor phase in the mineralization of aragonite or calcite by organisms.[7]

The structural differences between these carbonates can be easily distinguished by vibrational spectroscopy since the structures of aragonite and calcite are spectroscopically distinct and well documented.[8–11] However, this is not the case for vaterite: despite five different proposals for the crystal structure of vaterite,[12–17] a conclusive model is not yet available. Similarly, the correlation of the models for the crystal structure with the observed vibrational spectra for vaterite is still a matter of discussion. Most spectroscopic studies of vaterite focus on a comparison of the internal vibrational modes, and often only two or three of the proposed crystal structures are considered.[18–20]

Here, we present complete Raman spectra for biological, geological and synthetic vaterite in order to detect possible differences between samples of various origins and to provide reference spectra for further investigations. The spectroscopic results are evaluated in the light of all published crystal structures for vaterite and are aimed at gaining more detailed information about its crystallographic features. Additionally, the influence of magnesium on the widths of the Raman bands' full width at half-maximum (FWHM) is studied in order to detect a potential correlation between the magnesium content and the FWHMs, analogous to similar studies involving Mg-bearing calcite[21] and aragonite.[11,21]

Structurally, vaterite is often interpreted to be an endmember of the bastnäsite group, a solid solution series of calcium carbonates containing rare-earth elements and fluoride,[12–15] whereas other groups only assume bastnäsite ($(Ce,La,Y)[CO_3(F,OH)]$) and synchysite ($Ca(Ce,La)[(F,OH)|(CO_3)_2]$) as the endmembers of this series.[22,23] In this context, vaterite is interpreted as the rare-earth element and F-free endmember $CaCO_3$. The structure of this group of minerals could be described in terms of layers perpendicular to the hexagonal c axis[22,23] or, following Yang *et al.*,[24] as displaying two basic layers of CaO_8 and CeO_6F_3 polyhedra.

In order to pursue this possible link between the crystal structures of vaterite and minerals of the bastnäsite group, we present here new Raman spectroscopic data on parisite $Ca(Ce, La, Nd)_2[(CO_3)_3(F,OH)_2)]$ and discuss its relation to vaterite.

* *Correspondence to: U. Wehrmeister, Department of Geosciences and Earth System Science Research Centre, Johannes Gutenberg-Universität, Becherweg 21, D-55099 Mainz, Germany. E-mail: wehrmeis@uni-mainz.de*

a *Department of Geosciences and Earth System Science Research Centre, Johannes Gutenberg-Universität, Becherweg 21, D-55099 Mainz, Germany*

b *Department of Gemstone Research, Johannes Gutenberg-Universität, Becherweg 21, D-55099 Mainz, Germany*

Materials and Methods

Biogenic vaterite

Two Chinese freshwater cultured pearls (FWCPs) of *Hyriopsis cumingii* (samples China-4 and China-176) and one Japanese FWCP of *Hyriopsis schlegelii* crossed with *H. cumingii* from Lake Biwa (sample Biwa-11), all nonbeaded (i.e. without a bead nucleus) and between 7 and 9 mm in diameter, were selected for this study. The samples were cut in halves with a diamond-plated saw and polished with diamond paste on a copper plate. The cross sections that were studied by Raman spectroscopy revealed round vaterite areas close to the center of the pearls.[6]

Geological vaterite

Two samples from Bellerberg (Eifel Mountains, Germany) were selected. The rocks contain a mixture of minerals (e.g. ettringite $[Ca_6Al_2(SO_4)_3(OH)_{12}\cdot 26H_2O]$, calcite, aragonite and tobermorite $[Ca_5Si_6(O;OH)_{18}\cdot 5H_2O)]$ including white to dark yellow microcrystalline mineral aggregates of vaterite.

Synthetic vaterite

Synthetic vaterite samples were produced in collaboration with the Department of Inorganic and Analytical Chemistry at the University of Mainz. Vaterite was precipitated from a solution of $CaCl_2$ and polyaspartic acid in the presence of $(NH_4)_2CO_3$.[25] Magnesium was added as $MgCl_2$ to the $CaCl_2$ mother solution. The nominal Mg concentration was 2000 ppm (No. 061117.02), 4000 ppm (No. 071217.02) and 8000 ppm (No. 071217.04), respectively. In addition, an Mg-free sample was prepared (No. 060829.05). The actual Mg concentrations of the precipitated vaterite were analyzed *a posteriori* by XRF (x-ray fluorescence analysis) and yielded 482, 1266 and 1689 ppm Mg, respectively.

Parisite

The parisite sample was a crystal of gem quality from Muzo (Colombia, South America). In the famous emerald mine of Muzo, parisite occurs in paragenesis with marcasite, albite, calcite, pyrite, quartz and emerald.[26] Parisite has a rhombohedral lattice ($R3$) with lattice constants of $a = 7.1102(6)$ Å and $c = 83.834(8)$ Å for a superstructure with $c = 6c'$.[26]

Micro-Raman spectroscopy

All Raman spectra were recorded at room temperature using a Horiba Jobin Yvon LabRAM HR (high resolution) 800 spectrometer equipped with a Si-based charge-coupled device (CCD) detector (Peltier-cooled), an integrated Olympus BX41 optical microscope and an automatized x–y stage. A 50× long-distance objective (numerical aperture 0.55) and a slit width of 100 µm were chosen. The Rayleigh radiation was blocked using an edge filter, and the scattered light was dispersed by a grating with 1800 grooves/mm. The 532.21-nm line of a frequency-doubled Nd:YAG laser was used for excitation with a laser spot size of *ca* 2×2 µm. All spectra were recorded twice. The wavenumber accuracy is ± 0.5 cm^{-1} with a measured spectral resolution of 0.6 cm^{-1} (FWHM of the Rayleigh line). Spectra were calibrated using the 520.5 cm^{-1} band of a silicon wafer. Data acquisition and spectra treatment were carried out with the commercially available program LabSpec v4.02 (HORIBA Jobin Yvon GmbH). For all spectra, background subtraction and peak analysis were performed with the software OriginLabPro 7.5 equipped with an additional peak-fitting module.

For peak analysis, the different components of a spectrum were detected by overlapping Lorentzian curves optimized by successive iteration in the component number. All FWHMs were constrained between 10 and 50 cm^{-1} for the lattice modes, between 3 and 10 cm^{-1} for the ν_1 and the ν_4 Raman band and between 10 and 40 cm^{-1} for the ν_3 band of vaterite. The distance between the centers of consecutive peaks was constrained at a minimum of 2 cm^{-1}. Traces of calcite in synthetic vaterites and traces of aragonite in biogenic vaterites were fitted separately by fixing the corresponding wavenumber as well as the FWHMs: For calcite and aragonite, the position of the ν_1 band was fixed at 1085.5 cm^{-1} and the FWHMs with 5 and 2 cm^{-1}, respectively.

Chemical analysis

Trace and minor elements in different $CaCO_3$ polymorphs were measured using LA-ICP-MS (laser ablation inductively coupled plasma mass spectrometry) and using an Agilent 7500ce quadrupole ICP-MS coupled with a 213-nm Nd:YAG laser (New Wave Research UP213, wavelength 213 nm) for the sample ablation. Laser ablation parameters were as follows: spot diameter = 15 µm, frequency = 5 Hz, energy density = 6 J cm^{-2} and He as carrier gas. Plasma torch conditions were optimized so that the ThO/Th ratios were <0.5%. The NIST Standard Reference Material 612 glass (GeoReM preferred values: http://georem.mpch-mainz.gwdg.de/) was used for calibration. Data reduction was carried out with the commercial software GLITTER 4.0 (Macquarie University). Calcium, measured as ^{43}Ca, was used as the internal standard element for each analysis, with calcium concentrations measured by an electron probe microanalyzer (EPMA). One analysis took 120 s, during which time-resolved signals for background (60 s) and sample (60 s) were detected. Detection limits were generally significantly below 1 ppm (0.0001 µg g^{-1}). Reproducibility was evaluated by measuring the NIST Standard Reference Material 610 glass as an unknown, and amounts to less than 10% for the elements reported here.

Mg in synthetic vaterite powder was measured by XRF in a Philips MagiX PRO XRF instrument at the Department of Geosciences of the University of Mainz using standard procedures for carbonates. External standards used for calibration were the international standards and reference materials BCS368 (Dolomite), BCS393 (Limestone), GSR-6 (Limestone), KH-2 (Limestone) and NBS88A (Dolo-Limestone).[27]

Crystallography and band assignments

The vibrational spectra of carbonates can be divided in two regions. The region below 400 cm^{-1} contains bands that are due to motions comprising the complete unit cell, which are usually referred to as the lattice modes. The second region includes bands above 400 cm^{-1} which are caused by the internal modes of the molecular carbonate ion: 1064 cm^{-1} (ν_1), 879 cm^{-1} (ν_2), 1415 cm^{-1} (ν_3) and 680 (ν_4) cm^{-1}.[9,28,29]

All carbonate structures contain isolated CO_3^{2-} groups. The 'free' unperturbed CO_3^{2-} ion is trigonal planar with $\bar{6}\,2m$ (D_{3h}) point symmetry.[8,29] In calcite and aragonite, the point symmetry of the carbonate ion is lowered to 32 (D_3) and m (C_s), respectively[28] (see also Table 1). Vaterite is proposed to be pseudohexagonal and crystallized in the orthorhombic space group *Pbnm*[12,13] (standard setting: *Pnma*). In addition, four crystal structures with

Journal of RAMAN SPECTROSCOPY

Table 1. Crystal space groups and point-symmetries of the carbonate ion in five proposed structures of vaterite in Hermann-Mauguin and Schoenflies symbols (in parentheses). Calcite, aragonite and the 'free' carbonate ion are given for reference

	'Free carbonate ion'	Calcite [16,52]	Aragonite [53,54]	Vaterite [12,13]	Vaterite [15]	Vaterite [14]	Vaterite [16]	Vaterite [17]
Crystal system	Trigonal	Trigonal	Orthorhombic	Orthorhombic	Hexagonal	Hexagonal	Hexagonal	Hexagonal
Number of space group		167	62	62	194	194	182	179
Crystal space group		6 $R\bar{3}c$ (D_{3d}^6)	16 $Pmcn$ (D_{2h}^{16}) (standard setting: $Pnma$)	16 $Pbnm$ (D_{2h}^{16}) (standard setting: $Pnma$)	4 $P6_3/mmc$ (D_{6h}^4)	4 $P6_3/mmc$ (D_{6h}^4)	6 $P6_322$ (D_6^6)	3 $P6_522$ (D_6^6)
Site symmetry of the carbonate ion	$\bar{6}2m$ (D_{3h})	32(D_3)	m (C_S)	m (C_S)	2 mm (C_{2V})	m (C_S)	2 (C_2)	1 (C_1) and 2 (C_2)

hexagonal unit cells have been proposed: Kamhi[15] proposed a crystal structure for which a Raman spectrum with a doublet for ν_1, a singlet for ν_2 and triplets for ν_3 and ν_4 was predicted.[20] Meyer[14] proposed a crystal structure mainly in accordance with Kamhi's[15] structure, but with a different point symmetry of the carbonate ion. In contrast, for this proposed hexagonal structure by Meyer[14] quadruplets for ν_3 and ν_4 were predicted.[20] Lippmann[16] proposed a structure based on the high-temperature modification of $YbBO_3$, which gave rise to distinctly different predicted Raman bands: a triplet for ν_1, a doublet for ν_2 and five Raman bands for ν_3 and ν_4.[20] Lastly, Wang and Becker[17] gave account of a newly derived structure with space group $P6_522$ (Table 1). Although the differences between these crystal structures are significant, there are some general agreements: (1) The carbonate ions in vaterite are parallel to the *c* axis in contrast to aragonite and calcite (perpendicular to the *c* axis); (2) The disordering of the carbonate ions is notable; (3) Calcium atoms are in a hexagonal sublattice.

The mineral typically occurs in nature as microcrystalline aggregates, which makes single crystal analysis very difficult and could be one of the reasons for the lack of a conclusive determination of the crystal structure (Table 1).

In addition to the above studies, crystallographic structures for vaterite were modeled using Raman spectroscopic studies, but were not always compatible with the proposed structure for vaterite deducted from crystallographic studies. For example, some authors[18] concluded that none of the discussed structures for vaterite could be reconciled with the Raman spectra obtained in their study, whereas results of other studies[20] are compatible with the hexagonal structure proposed by Meyer.[14]

To underline the current lack of consensus in the literature, it should be noted that Anderson[19] gave a group theoretical analysis of the ν_1 $(CO_3)^{-[2]}$ vibration in vaterite and suggested the noncentrosymmetric hexagonal structure[16] (Table 1) to be the likeliest. This noncentrosymmetric structure was also favored by other authors.[30]

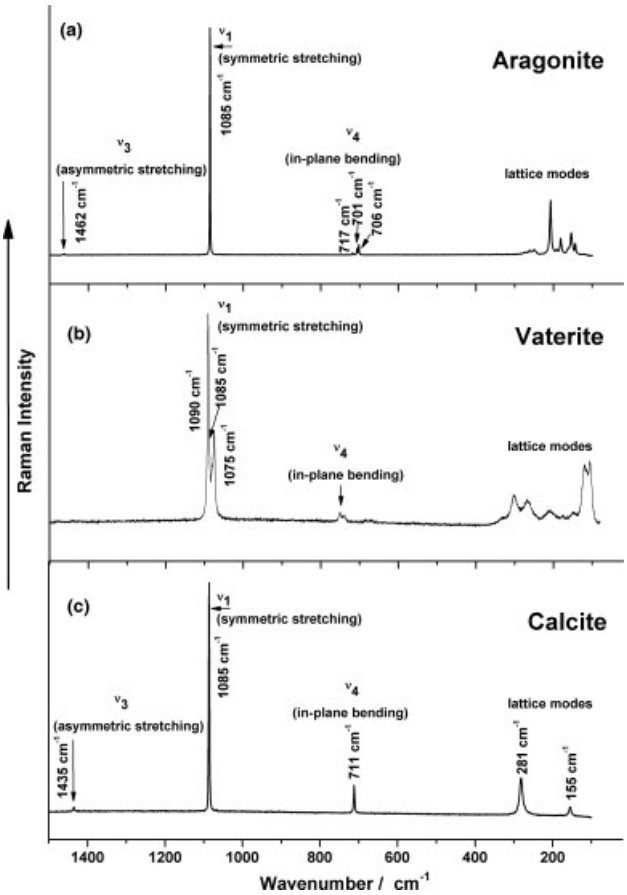

Figure 1. Raman spectra of aragonite (a), vaterite (b) and calcite (c). The spectra were obtained from the Raman database of the Department of Geosciences, Johannes Gutenberg- Universität, Mainz. The most intense ν_1 and the ν_4 band of the three polymorphs can be used to distinguish aragonite and calcite from vaterite clearly.

Results

Identification of $CaCO_3$ polymorphs

The most intense signals ν_1 (symmetric stretching) and ν_4 (in-plane bending) of the Raman spectra of the three carbonate polymorphs can be used to distinguish aragonite and calcite from vaterite (Table 2). Vaterite shows a typical triplet in the region between 1074 and 1091 cm^{-1}, whereas aragonite and calcite have a single band at *ca* 1085 cm^{-1} (see Table 2 and Fig. 1).

Raman scattering intensities in FWCPs are generally about 3 times higher in aragonite than in vaterite, while the luminescence

Table 2. Raman band positions (wavenumbers in cm^{-1}) and FWHMs (in cm^{-1}) of calcite and aragonite from literature and this study

	Lattice modes	ν_1 symmetric stretching	ν_2 out-of-plane	ν_3 asymmetric stretching	ν_4 in-plane bending
Calcite, synth.[21]	154 (6.2)	1085 (2.5)	n.a.	1434 (2.0)	711 (3.6)
	281 (10.1)				
Calcite, synth. (9.9 mole % $MgCO_3$)[21]	157 (14.7)	1087 (7.6)	n.a.	1438 (14)	714 (9.7)
	284 (18.3)				
Calcite, mineral[a]	154.9 (6.3)	1086 (1.9)	n.a.	1435.2 (3.9)	711.8 (2.7)
	281.3 (9.1)				
Aragonite[29]	113, 146, 155, 183, 193, 208,217, 222, 250, 263, 276, 287	1087	n.o.	1464	703
				1466	
Aragonite (cultured pearl)[11]	144, 153 (8.7), 180 (6.0), 190, 206 (7.4), 246, 261, 283	1085 (2.2)	n.o.	1462 (6.5)	701, 705
Aragonite (natural pearl)[11]	143, 153 (7.4), 180 (5.6), 190, 206 (6.8), 248, 259, 284	1085 (2.1)	852	1462 (5.0)	701, 705
Aragonite from *Philippine venus* seashell[55]	149 m, 178 w, 189 vw sh, 204 m, 246 w, 256 w, 270 w, 280 w	1083 vvs	–	1459 w	702 m
Aragonite, mineral[a]	144 (2.4), 154 (5.7); 163 (5.3), 181 (4.3), 192 (4), 208 (4.6), 249 (7.7), 262 (7.8), 272 (4.2), 276 (4.8), 285 (2.0)	1085 (1.3)	853	1462 (5.0)	702 (1.7)
			908		706 (2.0)
					718 (2.3)
Aragonite in FWCP sample China-176	143 (7.2), 153 (7.1), 162 (4.6), 181 (5.2), 207 (6.8), 249 (7.9), 261 (8.5), 275 (5.8), 284 (5.5)	1085 (1.7)	853 (1.6)	1462 (6.0)	701 (1.8)
			906 (8.0)		706 (2.2)
					717 (2.2)
Aragonite in FWCP sample Biwa-11	143 (6.1), 153 (7.8), 162, 180 (5.7), 191 (8.1), 206 (5.5), 214 (9.6), 248 (6.4), 273 (8.5), 284 (10)	1085 (1.7)	853 (1.9)	1462 (5.7)	701 (1.9)
			905		706 (2.2)
					717 (6.2)

n.a., not active; n.o., not observed; FWCP, short for freshwater cultured pearl; vw, very weak; w, weak; m, middle; sh, shoulder.
[a] Data for the minerals aragonite and calcite were obtained from the Raman data collection of the Department of Geosciences, Johannes Gutenberg-Universität, Mainz.

background relative to the main peak intensity is always higher in vaterite.[30–32] Because of the relatively high luminescence in most of the biological samples and the overlap with pigment peaks, the weak ν_2 and ν_3 Raman bands could not be measured, while in the region of the ν_4 Raman band only ambiguous peak positions could be observed.

Impurities of aragonite and calcite could be identified by a shoulder in the range of 1085 cm^{-1} and by a doublet at 701–705 cm^{-1} for aragonite and a peak at *ca* 712 cm^{-1} for calcite. In order to have a better comparison of the peak positions and FWHMs of the vaterite triplet, the calcite or aragonite shoulder (positions and FWHMs) was fixed during the fitting procedure.

Vaterite areas in the pearls often contain aragonite.[6] In contrast, traces of vaterite occurring in aragonite areas were not observed, and calcite has never been detected in our FWCP samples. Vaterite in geological samples contained trace aragonite and calcite impurities. Synthetic vaterite sample 060829.05 contained calcite, as detected by a peak in the ν_4 region between 701 and 718 cm^{-1} (Fig. 2) and a shoulder at *ca* 1086 cm^{-1} (Fig. 4). During the fitting procedures, these peak positions (711.5 and 1085.5 cm^{-1}) and FWHMs were fixed in order to obtain the peak components belonging only to vaterite.

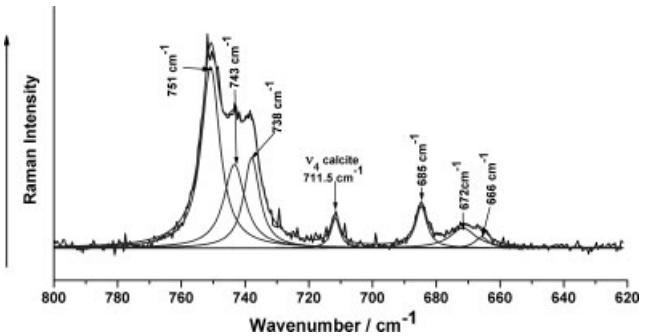

Figure 2. Raman spectra of the ν_4 region of synthetic vaterite sample 060829.05 (Mg-free). The peak at 711.5 cm^{-1} clearly indicates a calcite impurity. During the fitting procedure, the peak position and FWHM of the ν_4 band of calcite was fixed. The best result for fitting of the ν_4 region of vaterite was achieved for a decomposition of six peaks, three in the region between 650 and 700 cm^{-1} and three in the region between 720 and 780 cm^{-1}.

Spectroscopic analysis of vaterite

Lattice modes

The translational and rotational lattice modes appear in the low wavenumber region (*ca* 100–400 cm^{-1}) as very broad Raman

Journal of RAMAN SPECTROSCOPY

Table 3. Raman band positions (wavenumbers in cm^{-1}) and FWHM (cm^{-1}) of the lattice modes of vaterite from literature and from this study

Synthetic vaterite[30]	Biogenic vaterite from otolith of Coho Salmon (sample 1)[36]	Synthetic vaterite sample 060829.05	Synthetic vaterite sample 061117.02	Synthetic vaterite sample 071217.04	Vaterite, geological sample No.1	Vaterite, geological sample No.2	Vaterite, biogenic FWCP China-176	Vaterite, biogenic FWCP Biwa-11 spot 40	Spot 39
	106 (vs)	106 (15.5)	106 (16.0)	104 (18.5)	105	105			104 (20.6)
116.6 (10.0)	116 (sh)	120 (17.7)	120 (18.7)	120 (20.1)	119	119	118 (17.3)	120 (15.0)	121 (23.7)
130.3 (19.1)									
151.5 (16.2)	150 (s)	151 (20.4)	151 (22.0)	151 (30.6)	152 (15.0)	152 (16.4)	148 (21.6)	150 (22.5)	150 (30.3)
172.9 (21.1)	177 (w)	175 (25.2)	175 (26.7)	177 (36.6)	177 (17.4)	177 (19.7)	173 (24.1)	170 (25.9)	176 (38.2)
190.0 (10.5)									
208.4 (48.0)	210 (w)	210 (40.0)	210(40.1)	212 (45.0)	207 (25.7)	208 (29.0)	208 (35.8)	210 (34.2)	212 (45.0)
								236 (32.2)	
266.4 (35.4)	268 (m)	268 (32.8)	268 (34.0)	272 (44.2)	263 (34.3)	269 (35.0)	266 (34.8)	269 (36.7)	264 (42.6)
301.7 (22.2)	301 (s)	303 (21.1)	302 (22.1)	304 (25.8)	301 (19.7)	302 (19.1)	301 (22.0)	303 (31.6)	302 (29.1)
332.5 (31.3)	330 (s)	333 (20.3)	333 (18.6)	334 (20.1)	325 (24.2)	333 (18.1)	332 (19.0)	332 (16.8)	329 (23.6)

vs, very strong; sh, shoulder; s, strong; m, middle; w, weak.

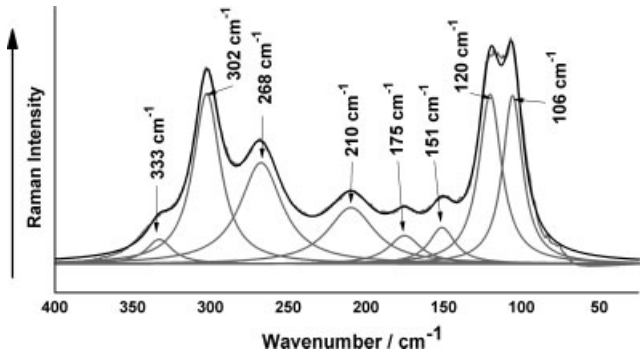

Figure 3. Raman spectrum of the lattice modes region of synthetic vaterite sample 061117.02. The best result of the fitting procedure was achieved for a decomposition of eight peaks.

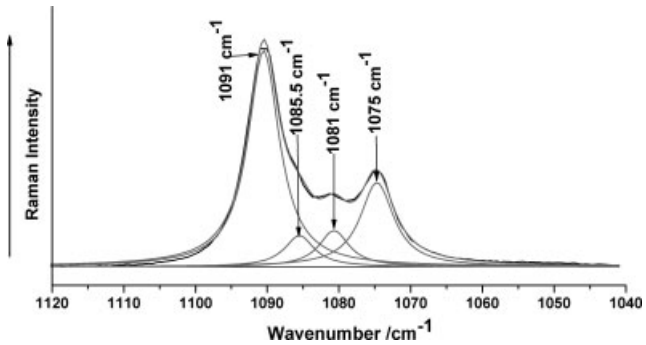

Figure 4. Splitting of the most intense Raman band ν_1 – the symmetric stretching mode of the carbonate ion in synthetic vaterite sample 060829.05. At 1085.5 cm^{-1} a calcite impurity is detected clearly. In this sample, the peak at 1085.5 cm^{-1} was identified as calcite, because in the same sample the ν_4 band of calcite was also detected (Fig.2). During the fitting procedure, the peak position and FWHM of the ν_1 band of calcite was fixed. The best result for fitting of the ν_1 band in vaterite was achieved for a decomposition of four peaks, whereas only three peaks belong to vaterite.

bands (Table 3, Figs 1 and 3), in contrast to the much narrower bands of calcite and aragonite in this region. These broad bands can be decomposed into eight distinct Raman bands (Table 3 and Fig. 3). Unfortunately, the very strong broad band in the region up to 150 cm^{-1} was too close to the limit of the edge filter to be decomposed correctly, which led to slightly different decompositions for peaks in the low wavenumber range in different samples. For synthetic and geological samples, this band decomposed clearly into two peaks (Figs 1 and 3 and Table 3), whereas in FWCPs in most cases only one peak was observed. The positions of six clearly decomposable peaks are in the range of 148–152, 170–177, 207–217, 263–272, 301–304 and 325–334 cm^{-1} with generally very broad FWHMs (Table 3) that are similar between biogenic, geological and synthetic samples: FWHMs of geological samples are in the range of 15–35 cm^{-1}, and FWHMs of synthetic and biological samples range from 15 to 45 cm^{-1}. Only in one FWCP, an additional peak at 236 cm^{-1} could be observed.

Internal modes of the CO_3^{2-} ion

Irrespective of the minerals' origin, Raman spectra of vaterite all show a triplet in the range between 1074 and 1091 cm^{-1} (ν_1 symmetric stretching mode) with bands between 1074 and 1075 cm^{-1}, 1079 and 1081 cm^{-1} and 1090 and 1091 cm^{-1} (Table 4). The most intense peak is at 1090–1091 cm^{-1}, with consecutively lower intensities for the peaks at 1075 and 1081 cm^{-1}, respectively (Fig. 4). In two synthetic samples (sample No. 060829.05 and No. 061117.02) we could confirm two Raman band positions at 873 and 877 cm^{-1} for the ν_2 out-of-plane bending mode, while only one Raman band at around 873 cm^{-1} could be observed in most of the other samples (Table 4)

The ν_3 band (antisymmetric stretching mode) can be resolved into five distinct bands in the synthetic and geological samples (Table 4). Because of an overlap with pigment peaks in the biological vaterites, the ν_3 band could not be measured in the pearls.

In synthetic and geological samples the ν_4 Raman band (in-plane bending mode) is observed to split into two different regions with differing intensities: one region in the area between 650 and 700 cm^{-1} and the other between 720 and 780 cm^{-1} (Fig. 2). Each region could be decomposed into three bands (Fig. 2 and Table 4). In FWCPs, only two to four bands in these regions could be observed.

Table 4. Raman band positions (wavenumbers in cm^{-1}) and FWHM (cm^{-1}) of the internal modes of the carbonate ion in vaterite from literature and from this study

Vaterite	ν_4	ν_2	ν_1	ν_3
Synthetic vaterite[30]	667.2 (8.4), 674.0 (9.7)	873.7 (5.5)	1075.0 (7.0)	1421.1 (21.1), 1440.9 (16.7), 1459.9 (26.8), 1480.4 (31.4)
	684.8 (6.4), 738.4 (7.9)	877.6 (2.5)	1081.4 (9.7)	1542.3 (35.1), 1555.0 (5.6)
	743.5 (7.3), 751.3 (8.7)	881 (8.5)	1090.9 (6.6)	
Biogenic vaterite from otolith of Coho Salmon (sample 1)[36]	685 (w), 740 (sh)	n.d.	1074 (s)	n.d.
	744 (sh), 751 (w)		1081 (w)	
			1090 (vs)	
Synth. vaterite sample 060829.05	666 (5.0), 672 (9.7)	873 (3.2),	1075 (5.6)	1421 (14.3), 1440 (16.4)
	685 (4.3), 738 (6.1)	877 (3.2)	1081 (5.1)	1456 (22.6), 1479 (27.0)
	743 (8.0), 751 (7.0)		1090 (5.3)	1557
Synth. vaterite sample 071217.04	667 (6.2), 672 (8.0)	873	1075 (6.7)	1421 (14.8), 1441 (17.0)
	685 (6.5), 739 (8.0)		1080 (5.9)	1460 (28.7), 1480 (30.9)
	745 (8.4), 752 (7.4)		1091 (6.2)	1554
Vaterite, geological sample No. 1	666 (5.1), 671 (4.3),	874 (9.0)	1075 (4.8)	1421 (12.4), 1438 (18.6)
	685 (3.7), 738 (4.8)		1079 (5.0)	1461 (14.5), 1479 (22.8)
	743 (7.0), 751 (6.5)		1090 (5.1)	1555
Vaterite, geological sample No. 2	668 (7.0), 673 (5.8),	875 (10.7)	1075 (4.9)	1440
	685 (4.1), 738 (4.7),		1081 (4.2)	1458
	743 (7.0), 751 (6.4)		1091 (4.5)	
Vaterite, biogenic FWCP-China-176	686 (4.5), 739 (4.9)	873	1074 (5.2)	n.a.
	745 (8.4), 753 (6.5)		1079 (5.4)	
			1090 (5.2)	
Vaterite, biogenic, FWCP-Biwa-11 spot 40	680	n.a.	1075 (4.7)	n.a.
	748		1079 (6.0)	
			1090 (5.1)	
Vaterite, biogenic FWCP-sample C spot 39	670	n.a.	1075 (5.5)	n.a.
	740		1081 (4.8)	
	751		1090 (4.9)	

n.a., Not analyzed because of an overlap with pigment peaks[31] or because of high luminescence.

Magnesium concentrations in vaterite and aragonite

In situ trace element measurements by LA-ICP-MS of aragonite and vaterite areas in FWCPs show that magnesium concentrations are variable but always significantly higher in vaterite (2984 $\mu g\ g^{-1}$) than in aragonite areas (1703 $\mu g\ g^{-1}$).[6,33,34] In order to detect a possible correlation of the magnesium content related to special features in the Raman spectra, spectra were obtained in aragonite and in vaterite regions in FWCP Biwa-11. Under identical analytical conditions, these spectra show different luminescence intensities with increasing magnesium content (Fig. 5(a) and (b)). The Raman spectra of the synthetic vaterite samples synthesized with differing Mg content show successively increasing FWHM with increasing Mg content both for the lattice modes and the ν_1 symmetric stretching mode (Tables 3 and 4).

Parisite

Similar to vaterite, the Raman spectrum for the parisite sample from Muzo is characterized by a splitting of the ν_1 band into three distinct peaks, which can be decomposed at 1081, 1091 and 1099 cm^{-1} (Fig. 6), whereas for the parisite samples from the Snowbird and F&S Mine only two peaks are reported.[35] The lattice mode region is characterized by 13 relatively intense peaks: at 100, 118, 128, 140, 158, 168, 199, 208, 250, 266, 305, 326 and 355 cm^{-1}.

The ν_4 (in-plane bending mode) is split into two different regions: one region in the area between 650 and 700 cm^{-1} and the other between 720 and 770 cm^{-1}. Each region could be decomposed into three discrete Raman bands (Fig. 6(c)). For the ν_2 and the ν_3 mode, three (866, 869 and 874 cm^{-1}) and four bands (1429, 1438, 1445 and 1459 cm^{-1}) could be identified, respectively.

Discussion

Band assignments and crystallography of vaterite

Eight discrete Raman bands in the lattice modes region were observed in all vaterite samples, irrespective of their origin (Table 3). These band positions are in relatively good agreement with previous studies.[30,36] Two bands at 130 and 190 cm^{-1}

Journal of RAMAN SPECTROSCOPY

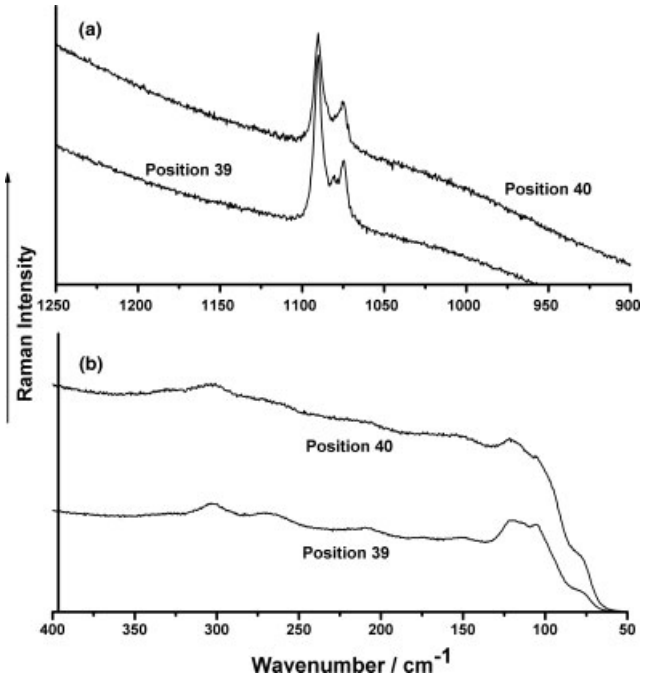

Figure 5. Raman spectra obtained from two different spots in a vaterite area of freshwater cultured pearl Biwa-11. The magnesium content quantified at spot 39 is 1704 ppm and at spot 40 is 2957 ppm (data measured by LA-ICP-MS, analytical uncertainty is 10%). The Raman spectra obtained in the area of ν_1 (a) and in the region of the lattice modes (b) suggest the dependence of luminescence on the increasing magnesium content.

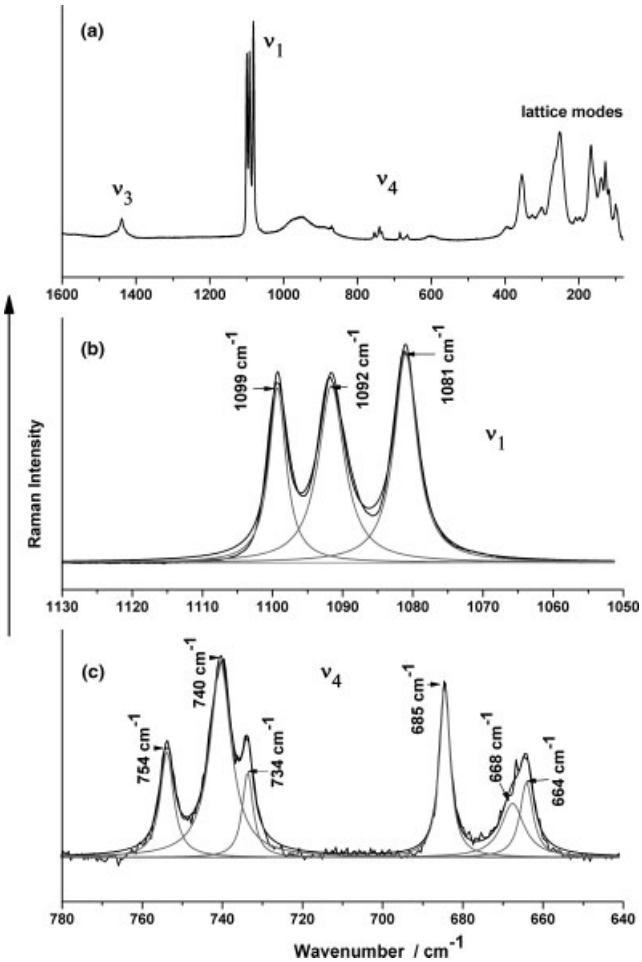

Figure 6. Raman spectra of parisite (a). Splitting of the most intense Raman band ν_1 – the symmetric stretching mode of the carbonate ion in parisite – into three distinct bands (b). Splitting of ν_4 – the in-plane bending mode of the carbonate ion in parisite – into six distinct Raman bands (c).

reported in the study of Hollett[30] could not be confirmed in our study nor by Gauldie *et al*.[36] The band observed at 190 cm^{-1} is reported to belong to aragonite (Table 2).

The measured high-resolution spectra show a ν_1 triplet of the internal modes of the CO_3^{2-} ion (Figs 4 and 1(b)), which is in good agreement with those in the studies of Gauldie and Sharma[36] and Hollett,[30] whereas other groups reported only a doublet for the ν_1 Raman signal of the carbonate ion in vaterite.[18,20] A thorough examination of the published Raman spectra, however, implies that the absence of the third and smallest band in the ν_1 position may be due to the lower resolution in these studies.

The splitting of the ν_1 peak was taken as an indication of the molecular symmetries of the carbonate ion and the number of nonidentical carbonate groups,[8,18,30] implying that the proposed vaterite crystal structures with equivalent sites for the carbonate ion could not be correct.[18] Notably, the first crystal structure with different point symmetries for the CO_3^{2-} ions was proposed by Wang and Becker[17] in 2009.

Two peaks in the area between 872 and 878 cm^{-1} were detected in the ν_2 region (Table 4). Results for this area are rather divergent: Hollett,[30] for example, observed three peaks; Gabrielli *et al*.[20] gave account of a single peak at 874 cm^{-1}; while other groups[18,36] observed none in this region.

For the ν_3 region, our study clearly indicates four peaks in the area between 1421 and 1480 cm^{-1} in agreement with the observations of Hollett.[30] In that study, the author reported two peaks at 1542 and 1555 cm^{-1}, whereas our results show a very weak, relatively broad band around 1555 cm^{-1}.

Lastly, the splitting of the ν_4 region into two segments with three components each (Fig. 2 and Table 4) is in a good agreement with the result of Hollett,[30] whereas other studies observed only four distinct bands.[20,36] According to Nakamoto *et al*.,[28] the in-plane bending mode splits into two components as the carbonate ion become distorted from regular plane symmetry.[37] The three Raman bands of each segment are believed to correspond to at least three structurally independent carbonate groups.[30]

In general, the lattice modes as well as the internal modes of the carbonate ion of vaterite have large FWHMs of 15–44 and 3–31 cm^{-1}, respectively (Tables 3 and 4), which are considerably larger than those of aragonite or calcite (Table 2). This gives evidence that the crystal structure is not as well crystallized as it is in the case for aragonite and calcite.

The structure proposed by Lippmann[16] predicts a triplet[30,36] for the ν_1 Raman band,[20] as is confirmed in our study, suggesting at least three nonequivalent carbonate ions in the unit cell.

The influence of magnesium

An increase of the Mg content in synthetic calcite is known to cause a slight shift of the Raman band positions to higher wavenumbers in addition to a systematic increase in FWHMs.[21] (For example, a FWHM of 12.4 cm^{-1} and a Raman band position of 1088 cm^{-1} for synthetic magnesium calcite with 25 mol% $MgCO_3$ was reported.)[21]

Although vaterite accommodates orders of magnitudes less magnesium in its crystal lattice, an analogous trend for its FWHMs as for calcite can be observed. With increasing Mg concentrations, the synthetic vaterite samples show increasing FWHMs in the region of the lattice modes (Table 3) and the three ν_1 bands (Table 4), while no change in luminescence was detected. In contrast, biogenic vaterite with higher magnesium content shows higher luminescence intensity (Fig. 5), while the FWHMs are unchanged. It is often proposed that the formation of biological vaterite may be related to the presence of inorganic ions[38–40] or organic molecules[6,33,34,41] that act as stabilizers. Magnesium is also an abundant component of aspartic and glutamic-rich polypeptides,[42] which are the most common amino acids in glycoproteins and carry out important control functions during biomineralization.[43] *In situ* element concentration measurements support this. Higher magnesium concentrations within vaterite are found in the organic-rich growth rings. This suggests that considerable amounts of Mg may be present as Mg organic species[31,44,45] rather than in the crystal lattice of vaterite. This may also explain the fact that synthetic vaterite reaches Mg saturation roughly at around 2000 ppm[45] (Materials and methods), while much higher values are observed in biominerals.[46,47]

Similarities of the Raman spectra of vaterite and parisite

The structural differences of the carbonates are manifest in their Raman spectra: e.g. all carbonates with calcite structure show a similar spectrum, whereas the shifts of the peak positions depend on the radius of the cations of the structure.[8,48] As opposed to the spectra of aragonite, calcite and bastnäsite-(Ce), which show only one distinct band for the symmetric stretching vibration (ν_1), this band in vaterite is a triplet in the range of 1074–1091 cm^{-1}.

There are several other carbonates with this characteristic splitting of the symmetric stretching vibration (ν_1): e.g. α-$Na_2Ca(CO_3)$, hydroxylbastnäsite, synchysite-(Ce), northupite and parisite-(Ce).[35,49,50] On comparing the Raman data of vaterite and parisite (Fig. 6), the following similarities become obvious:

1. The most intense band ν_1 splits into three distinct Raman bands in the range of 1074–1091 and 1081–1099 cm^{-1} for vaterite and parisite, respectively (Figs 1, 2 and 6).
2. In most of the vaterite samples, only one Raman band at around 874 cm^{-1} could be determined for the ν_2 out-of-plane bending mode. Only in some cases, an additional band at 877 cm^{-1} could be observed. For parisite, three bands in the range of 866–874 cm^{-1} were determined.
3. For the ν_3 mode, a splitting into two different regions was observed in the vaterite samples: one region between 1420 and 1481 cm^{-1}, displaying four distinct Raman bands; and an additional, very weak broad band at *ca* 1555 cm^{-1}. For parisite, four distinct Raman bands could be observed in the range between 1429 and 1459 cm^{-1}.
4. The splitting of the ν_4 band into two different regions was observed, with three Raman bands each: one region in the area between *ca* 650 and 690 cm^{-1} and the other between *ca* 720 and 780 cm^{-1} for vaterite and parisite (Figs 2 and 6).
5. In the lattice modes region, 13 distinct Raman bands were determined for parisite with a maximum of 22 cm^{-1} for the FWHMs, whereas for vaterite 8 Raman bands could be decomposed with FWHMs up to 45 cm^{-1}.

Following the pioneering works of Meyer,[12–14] Kamhi[15] and McConell,[51] vaterite could be seen as the endmember of the solid solution series of the rare-earth–calcium fluoride carbonates (bastnäsite–parisite–röntgenite–synchysite). In general, minerals of this series are characterized by a number of imperfections, namely twinning, syntactic intergrowth, stacking faults, and chemical disorder, and are most often reported to occur in paragenesis with other mineral phases.[22]

Because of the conspicuous similarities between the Raman spectra of parisite-(Ce) and vaterite, especially the internal modes of the carbonate ion, it is suggested that the geometries of the carbonate layers are essentially similar and that there may be at least three structurally nonequivalent carbonate groups.[50] Furthermore, in consideration of the concordance of their Raman spectra, the similarities of the point symmetries of the carbonate group in vaterite and the stacking sequence of the carbonate group layers have to be reviewed. It could be assumed that the (CO_3) layers are generally similar, whereas no information of the stacking sequence is available. The overall similarity between the Raman spectra of this group of carbonates opens the possibility that there may also exist different polytypes of vaterite, possibly affected by syntactic intergrowth, stacking faults, layer shifts and crystal growth, along with other mineral phases causing the difficulties in obtaining exact crystallographic data.

Conclusions

Raman spectra of aragonite in FWCPs show the same Raman band positions as reported in the literature for synthetic, biological and mineral samples. The FWHMs of the Raman bands in the pearl samples are in general higher. Overall, the small FWHMs indicate a well-ordered crystal structure of aragonite in FWCPs.

The Raman band position and FWHMs of vaterite in all samples are generally in good agreement, independent of their origin. The characteristic features of the Raman spectrum of vaterite observed in this study are (1) the presence of at least eight relatively broad bands in the region of the external lattice modes; (2) a splitting of the most intense band ν_1 into three distinct bands; (3) activation and splitting of ν_2; and (iv) splitting of both ν_3 and ν_4 into two different regions. The FWHMs of the lattice modes are comparatively high (15–45 cm^{-1}), while the FWHMs of the most intense Raman band – the ν_1 symmetric stretching mode – are distinctly narrower (e.g. for the band at 1090 cm^{-1} from 4.5 to 6.7 cm^{-1}), supporting earlier studies. In comparison to the FWHMs of aragonite, those of vaterite are higher, implying that the crystal structure of the latter is not as well ordered but is possibly affected by stacking faults, layer shifts or syntactic intergrowth irregularities, making it difficult to determine the crystal structure.

In situ measurements of aragonite and vaterite areas in FWCPs by LA-ICP-MS show that magnesium concentrations are significantly higher in vaterite than in aragonite areas.[6,45] Raman data obtained at the same spots in the pearls show increasing luminescence intensities with increasing Mg content in the vaterite areas.

The FWHMs of the lattice modes and the ν_1 bands of synthetic vaterites increase with increasing magnesium content and indicate that at least some of the Mg ions are incorporated in the crystal lattice of vaterite.

By collating the Raman spectrum of vaterite with the spectra of parisite, definite similarities due to the internal modes of the carbonate ion are obvious, pointing towards the possibility of at least three structurally independent carbonate groups in the unit cell of vaterite. Furthermore, Raman spectroscopy supports that

the carbonate ion has the same symmetry and that carbonate group layers are similar to those of parisite-(Ce). It is reasonable to suggest that the stacking of the carbonate group layers in the structure of vaterite may result in a lower symmetry. These findings define an important base for future models of the crystal structure of vaterite.

Acknowledgements

This work was financially supported by the Earth System Science Research Center (Geocycles) funded by the state of Rheinland-Pfalz, Germany, and is publication number 623. The authors thank N. Loges for the production of the synthetic vaterite samples used in this study. Two anonymous reviewers helped to improve this manuscript, which is gratefully acknowledged.

References

[1] M. R. Snow, A. Pring, P. Self, D. Losnic, J. Shapter, *Am. Mineral.* **2004**, *89*, 1353.
[2] H. Y. Ma, I.-S. Lee, *Mater. Sci. Eng. C* **2006**, *26*, 721.
[3] L. Qiao, Q. L. Feng, *J. Cryst. Growth* **2007**, *304*, 253.
[4] L. Qiao, Q. L. Feng, Z. Li, *Cryst. Growth Des.* **2007**, *7*(2), 275.
[5] L. Qiao, Q. L. Feng, Y. Liu, *Mater. Lett.* **2008**, *62*(12–13), 1793.
[6] U. Wehrmeister, D. E. Jacob, A. L. Soldati, T. Häger, W. Hofmeister, *J. Gemmol.* **2007**, *30*(7/8), 399.
[7] B. Hasse, H. Ehrenberg, J. C. Marxen, W. Becker, M. Epple, *Chem. Eur. J.* **2000**, *6*, 3679.
[8] H. H. Adler, P. F. Kerr, *Am. Mineral.* **1963**, *48*, 124.
[9] B. E. Scheetz, W. B. White, *Am. Mineral.* **1977**, *62*, 36.
[10] R. Frech, E. C. White, *Spectrochim. Acta* **1980**, *36A*, 915.
[11] J. Urmos, S. K. Sharma, F. T. MacKenzie, *Am. Mineral.* **1991**, *76*, 614.
[12] H. J. Meyer, *Angew. Chem.* **1959**, *21*, 678.
[13] H. J. Meyer, *Fort. Mineral.* **1960**, *38*, 186.
[14] H. J. Meyer, *Z. Kristallogr.* **1969**, *128*, 183.
[15] S. Kamhi, *Acta Crystallogr.* **1963**, *16*, 770.
[16] F. Lippmann, *Sedimentary Carbonate Minerals*, Springer Verlag: New York, **1973**.
[17] J. Wang, U. Becker, *Am. Mineral.* **2009**, *94*, 380.
[18] G. Behrens, L. Kuhn, R. Ubic, A. Heuer, *Spectrosc. Lett.* **1995**, *28*, 983.
[19] A. Anderson, *Spectrosc. Lett.* **1996**, *29*, 5.
[20] C. Gabrielli, R. Jaouhari, S. Joiret, G. Maurin, *J. Raman Spectrosc.* **2000**, *31*, 497.
[21] W. D. Bischoff, S. K. Sharma, F. T. MacKenzie, *Am. Mineral.* **1985**, *70*, 581.
[22] G. Donnay, D. H. Donnay, *Am. Mineral.* **1953**, *38*, 932.
[23] J. van Landuyt, S. Amelinckx, *Am. Mineral.* **1975**, *60*, 351.
[24] Z. Yang, K. Tao, P. Zhang, *N. Jb. Mineral. Mh.* **1998**, *1*, 1.
[25] N. Loges, K. Graf, L. Nasdala, W. Tremel, *Langmuir* **2006**, *22*, 3073.
[26] U. Henn, H. von Platen, W. Hofmeister, H. Bank, *N. Jb. Miner. Mh.* **1992**, *6*, 258.
[27] K. Govindaraju, *Geostandards Newsl.* **1989**, *13*, 114, Special Issue.
[28] K. Nakamoto, J. Fujita, H. Naka, M. Obayashi, *J. Am. Chem. Soc.* **1957**, *79*, 4904.
[29] W. B. White, *Mineralogical Society Monograph 4* (Ed.: V. C. Farmer), Mineralogical Society: London, **1974**, p 227.
[30] M. J. Hollett. The Spectroscopic Analysis of Vaterite and Other Forms of Calcium Carbonate, Master of Science Thesis, Department of Chemistry St. John's, Newfoundland, Memorial University of Newfoundland, **2000**.
[31] A. L. Soldati, D. E. Jacob, U. Wehrmeister, T. Häger, W. Hofmeister, *J. Raman Spectrosc.* **2008**, *39*, 525.
[32] S. Karampelas, E. Fritsch, J. Y. Mevellec, J. P. Gauthier, S. Sklavounos, T. Soldatos, *J. Raman Spectrosc.* **2007**, *38*, 217.
[33] D. E. Jacob, A. L. Soldati, U. Wehrmeister. 17th annual V.M. Goldschmidt conference, Cologne, **2008**, abstracts 3, 5016doc.
[34] D. E. Jacob, A. L. Soldati, R. Wirth, J. Huth, U. Wehrmeister, W. Hofmeister, *Geochim. Cosmochim. Acta* **2008**, *72*(22), 5401.
[35] R. L. Frost, M. J. Dickfos, *J. Raman Spectrosc.* **2007**, *38*, 1516.
[36] R. W. Gauldie, S. K. Sharma, E. Volk, *Comp. Biochem. Physiol. A* **1997**, *118*, 753.
[37] R. L. Frost, S. Bahfenne, *J. Raman Spectrosc.* **2009**, *40*, 360.
[38] N. Nassrallah-Aboukais, A. Boughriet, L. Gegembre, A. Aboukais, *J. Chem. Soc., Faraday Trans.* **1998**, *94*, 2399.
[39] V. Noethig-Laslo, L. Brecevic, *J. Chem. Soc., Faraday Trans.* **1998**, *94*, 2005.
[40] L. Brecevic, V. Noethig-Laslo, D. Kralj, S. Popovit, *J. Chem. Soc., Faraday Trans.* **1996**, *92*(6), 1017.
[41] G. Falini, S. Fermani, S. Vanzo, M. Miletic, G. Zaffino, *Eur. J. Inorg. Chem.* **2005**, 162.
[42] T. Dudev, J. Cowan, C. Lim, *J. Am. Chem. Soc.* **1999**, *121*, 7665.
[43] Y. Levi-Kalisman, G. Falini, L. Addadi, S. Weiner, *J. Struct. Biology.* **2001**, *135*, 8.
[44] B. R. Schöne, Z. Zhang, D. P. Gillikin, D. E. Jacob, T. Tütken, D. Garbe-Schönberg, T. McConnaughey, A. Soldati, *Geochem. J.* in press.
[45] A. L. Soldati, D. E. Jacob, U. Wehrmeister, W. Hofmeister, *Mineral. Mag.* Special Issue on Biominerals **2008**, *72*, 577.
[46] S. Y. Kwak, E. DiMasi, Y. J. Han, J. Aizenberg, I. Kuzmenko, *Cryst. Growth Des.* **2005**, *5*(6), 2139.
[47] J. England, M. Cusack, M. R. Lee, *Lethaia* **2007**, *40*, 2.
[48] C. V. Farmer, A. N. Lazarev, *Mineralogical Society Monograph 4* (Ed.: V. C. Farmer), Mineralogical Society: London, **1974**, p 51.
[49] M. E. Böttcher, C. Reutel, *J. Raman Spectrosc.* **1996**, *27*, 859.
[50] H. Yang, R. F. Dembrowski, P. G. Conrad, R. T. Downs, *Am. Mineral.* **2008**, *93*, 698.
[51] J. D. C. McConnell, *Mineral. Mag.* **1960**, *32*, 535.
[52] A. J. Skinner, J. P. LaFemina, H. J. F. Jansen, *Am. Mineral.* **1994**, *79*, 205.
[53] J. P. R. DeVilliers, *Am. Mineral.* **1971**, *56*, 758.
[54] A. DalNegro, L. Ungaretti, *Am. Mineral.* **1971**, *56*, 768.
[55] F. Z. Zakaria, J. Mihaly, I. Sajo, R. Katona, L. Hajba, F. A. Aziz, J. Mink, *J. Raman Spectrosc.* **2008**, *39*, 1204.